AGU PUBLICATIONS

Geophysical Research Letters

RESEARCH LETTER
10.1002/2014GL061357

Key Points:
- Sandy underwent tropical to extratropical transition before its landfall
- The storm track was largely determined by synoptic atmospheric circulation
- Ocean coupling was not as important because the storm was moving fast

Correspondence to:
R. He,
rhe@ncsu.edu

Citation:
Zambon, J. B., R. He, and J. C. Warner (2014), Tropical to extratropical: Marine environmental changes associated with Superstorm Sandy prior to its landfall, *Geophys. Res. Lett.*, *41*, doi:10.1002/2014GL061357.

Received 31 JUL 2014
Accepted 19 NOV 2014
Accepted article online 25 NOV 2014

Tropical to extratropical: Marine environmental changes associated with Superstorm Sandy prior to its landfall

Joseph B. Zambon[1], Ruoying He[1], and John C. Warner[2]

[1]Department of Marine, Earth and Atmospheric Sciences, North Carolina State University at Raleigh, Raleigh, North Carolina, USA, [2]United States Geological Survey, Woods Hole, Massachusetts, USA

Abstract Superstorm Sandy was a massive storm that impacted the U.S. East Coast on 22–31 October 2012, generating large waves, record storm surges, and major damage. The Coupled Ocean-Atmosphere-Wave-Sediment Transport modeling system was applied to hindcast this storm. Sensitivity experiments with increasing complexity of air-sea-wave coupling were used to depict characteristics of this immense storm as it underwent tropical to extratropical transition. Regardless of coupling complexity, model-simulated tracks were all similar to the observations, suggesting the storm track was largely determined by large-scale synoptic atmospheric circulation, rather than by local processes resolved through model coupling. Analyses of the sea surface temperature, ocean heat content, and upper atmospheric shear parameters showed that as a result of the extratropical transition and despite the storm encountering much cooler shelf water, its intensity and strength were not significantly impacted. Ocean coupling was not as important as originally thought for Sandy.

1. Introduction

Tropical cyclones (TCs) and extratropical cyclones represent large, discrete events that have dramatic effects on the marine environment. As considerably more people and property have aggregated to the shoreline in recent decades, the damage caused by these intense storms will continue to increase [*Emanuel*, 2005]. These impacts are not only dependent upon strength (represented by maximum 10 m wind) and intensity (represented by minimum sea level pressure) of the storm but also storm size [*Merrill*, 1984; *Hill and Lackmann*, 2009]. On 22–31 October 2012, the U.S. East Coast was under the direct impact of a massive storm. Record storm surges were observed in highly populated areas of New Jersey, New York, and Connecticut. Combining devastating flooding with hurricane-force winds, the massive hurricane and extratropical storm that became known as Superstorm Sandy (hereafter, Sandy) was the second-costliest cyclone on record to impact the United States [*Blake et al*., 2013]. Sandy made landfall in New Jersey, U.S., approximately 2 h after becoming an extratropical system [*Blake et al*., 2013]. The distinction between tropical and extratropical storm proved to be extremely important for claims made to insurance companies. Thousands of families found their insured homes not covered as they were victims of a "flood" and not a "hurricane" [*Smith*, 2012].

Sandy has an interesting synoptic history. National Hurricane Center (NHC) forecasts issued at 03Z on 27 October described Sandy as having characteristics of hybrid cyclone, with the appearance of an occluded low but with a deep warm core and no significant surface temperature gradient [*Beven*, 2012]. *Galarneau et al*. [2013] perform an investigation into the extratropical transition of this storm, which begins at 00Z 29 October as Sandy interacted with a polar trough and completed near 21 Z on 29 October. In this study, we utilized the Coupled Ocean-Atmosphere-Wave-Sediment Transport (COAWST) modeling system [*Warner et al*., 2010] to simulate Sandy and its impact on the ocean and wave environments as it made landfall in the northeast U.S. The COAWST modeling system has been utilized in the past to examine intense hurricanes [*Warner et al*., 2010; *Olabarrieta et al*., 2012], strong Nor'easters [*Nelson and He*, 2012]. The purpose of this case study is to utilize the COAWST model to examine the effects the atmosphere, ocean, and wave environments had on Sandy as it completed tropical to extratropical transition.

2. Model Configuration

COAWST couples three state-of-the-art numerical models representing the ocean, atmosphere, and wave environments. These models are the Regional Ocean Modeling System (ROMS) [*Haidvogel et al*., 2008], the

Weather Research and Forecasting (WRF) model [*Skamarock et al*., 2005], and the Simulating Waves Nearshore (SWAN) model [*Booij et al*., 1999], respectively. For the WRF model, we utilized a TC-following nested atmospheric grid to resolve the inner eyewall processes of Sandy [*Hill and Lackmann*, 2009; *Gopalakrishnan et al*., 2012]. The outer grid encompassed the entire U.S. East Coast with a grid spacing of 9 km, while the inner grid was scaled down to 3 km. The WRF model time step was defined as 24 s on the outer grid and 8 s on the inner grid. Grid-resolved precipitation on both grids was computed using the WRF Single-Moment six-class microphysics scheme (WSM-6) from *Hong and Lim* [2006]. This first-order microphysics scheme features water vapor, cloud water, cloud ice, rain, snow, and graupel. On the 9 km outer grid, the Kain-Fritsch CP scheme [*Kain*, 2004] was used to parameterize precipitation processes on a subgrid scale. For the inner grid, the 3 km mesh was able to resolve precipitation adequately and no cumulus parameterization was necessary. Longwave and shortwave radiation physics were computed using the Rapid Radiative Transfer Model [*Mlawer et al*., 1997] and the [*Dudhia*, 1989] scheme, respectively. The Eta surface layer scheme [*Janjić*, 1996, 2002] based on similarity theory [*Monin and Obukhov*, 1954] physics option was used along with the Noah land surface model [*Chen and Dudhia*, 2001] for both grids. The Mellor-Yamada-Janjić turbulent kinetic energy planetary boundary layer model [*Mellor and Yamada*, 1982; *Janjić*, 1990, 1996, 2002] was called every time step on both WRF domains. The initial and boundary conditions for the WRF model are derived from the 1° National Centers for Environmental Prediction (NCEP) Final (FNL) Operational Model Global Tropospheric Analyses [*National Centers for Environmental Prediction*, *National Weather Service*, *NOAA*, *U.S. Department of Commerce*, 2000]. The product was used to initialize WRF approximately 35 h before landfall (12Z 28 October) with boundary conditions updated every 6 h.

The ROMS/SWAN domain is spatially collocated with the WRF outer domain, with the exception of small lateral boundaries placed on all sides to ensure WRF forcing exists for the entire ROMS/SWAN domain. This domain features grid spacing of 7 to 10 km, small enough to resolve atmospheric forcing from tropical cyclones [*Halliwell et al*., 2011]. The ROMS domain has 36 stretched, terrain-following vertical coordinates, with finer grid spacing used closer to the ocean surface. A 25 s baroclinic time step was used. We followed the scheme of *Marchesiello et al*. [2001], whereby Orlanski-type radiation conditions were used in conjunction with relaxation (with time scale of 0.5 days on inflow and 10 days on outflow) to downscale daily tracer (salinity and temperature) and 3-D velocity fields of global HYbrid Coordinate Ocean Model with Naval Research Lab Coupled Ocean Data Assimilation (HYCOM/NCODA) [*Chassignet et al*., 2007] solutions, which also provided the initial ocean conditions. For the free surface and depth-averaged velocity boundary conditions, we adopted the method of *Flather* [1976] with the external values also defined by daily HYCOM/NCODA. Our ROMS setup used a [*Mellor and Yamada*, 1982] method to compute vertical turbulent mixing, as well as the quadratic drag formulation for the bottom friction specification.

In the SWAN setup, we use the same spatial grid as the ROMS model where directional space was utilized with 36 directional bins and 24 frequency bins between 1 s and 25 s. Nonlinear quadruplet wave interactions were activated in the model. Wave bottom dissipation was parameterized using the *Madsen et al*. [1988] formulation, with an equivalent roughness length scale of 0.05 m. The depth-induced breaking constant, i.e., the wave height to water depth ratio for breaking waves, was set to 0.73. Wind-wave growth was generated using the Komen formulation [*Komen et al*., 1984]. A backward-in-space, backward-in-time advection scheme was used for iteration. SWAN was initialized in stationary mode with surface forcing provided by WRF. Boundary conditions were updated every 3 h from solutions of the global WaveWatch 3 (WW3) model (http://polar.ncep.noaa.gov/waves/index2.shtml).

We found that with the wave coupling, treatment of the surface roughness length had a definite effect on the maximum wind speed derived in the simulations and is clearly an area needing more research and refinement. Here we chose to use the *Taylor and Yelland* [2001] parameterization to calculate surface roughness length:

$$\frac{z_0}{H_s} = A_1 \left(\frac{H_s}{L_p}\right)^{B_1}$$

where H_s is the significant wave height (in m) and L_p the wave length (in m). A_1 and B_1 are constants calculated in *Taylor and Yelland* [2001] to be 1200 and 4.5 (both are dimensionless values), respectively. The COAWST system provides two other parameterizations for surface roughness: that in *Oost et al*. [2002] and in

Drennan et al. [2005]. Our sensitivity experiments show that the [*Taylor and Yelland*, 2001] parameterization provided the best simulation overall among the three, based on comparisons to NHC track, intensity, strength, and in situ buoy comparisons of SST and wave heights (not shown).

Our COAWST hindcast for Sandy initialized at 12Z 28 October 2012 and ran through 00Z 3 November 2012 to cover the relaxation period after storm passage, and for in situ data comparisons.

3. Experiment Design

Four experiments were performed, with increasing complexity, to explore the ocean-wave-atmosphere dynamics during Sandy. The first experiment (WRF-Static) utilized a WRF-only simulation with a sea surface temperature (SST) condition that was unchanged after initialization. The second experiment (WRF-OML) featured a one-dimensional Ocean Mixed Layer (OML) model [*Pollard et al*., 1972] integrated into WRF [*Davis et al*., 2008]. For the WRF-OML experiments, we utilized a $-0.14°C\,m^{-1}$ lapse rate and a 50 m mixed layer throughout the entire ocean domain. The third experiment (two-way) featured coupling between the WRF and ROMS models, such that the SST was passed from ROMS to WRF and sea surface stresses (τ) and net heat flux were passed from WRF to ROMS. The fourth experiment (three-way) included full coupling between the WRF, ROMS, and SWAN models and allows WRF to pass winds at 10 m above the sea surface directly to SWAN, which used them in the computation of significant wave height, average wavelength, and relative peak period; these were then passed back to WRF and ROMS. Surface wave direction, bottom wave period, bottom orbital velocity, percentage of breaking waves, and dissipation energy also were transferred from SWAN to ROMS. Sea surface height (SSH) and east and north currents computed as a vertical distribution of the current profile based on the method of *Kirby and Chen* [1989] were passed from ROMS to SWAN.

4. Results

4.1. Comparisons of Sandy's Track, Intensity, and Strength

A comparison of numerical simulations of Sandy's track, intensity (minimum Sea Level Pressure; SLP), and strength (maximum 10 m wind) to the National Hurricane Center's (NHC) best track (Verification) [*Blake et al*., 2013] shows that all experiment results are similar to Verification through landfall (approximately hour 34 of the simulations; Figure 1). Sandy maintained a similar track in all simulations (Figure 1a) before its landfall. Twelve hours after landfall, the simulated tracks began to diverge. This is in part a consequence of the tracking algorithm, which follows the location of lowest central pressure whereas the best track locates the center of storm. As Sandy moved inland, the storm became disorganized, and the center of circulation was not consistent with the location of lowest central pressure.

The comparison of the simulated intensities (minimum central pressure, unit: hPa) against Verification likewise shows similar values (Figure 1b). The correlation coefficient (r) and root-mean-square error (RMSE) of minimum SLP (Table 1) indicate that the three-way coupled simulation had the best correlation (0.938) and significantly reduced RMSE (6.9 hPa) among all cases. The worst performing simulation was WRF-OML, with r of 0.91 and RMSE of 9.0 hPa.

Greater variance appeared between the simulated strength (maximum 10 m wind speed, unit: $m\,s^{-1}$) of all four experiments and Verification (Figure 1c). The wave-uncoupled models all yielded similar results with the greatest differences occurring with the wave-coupled experiment, a consequence of the parameterization of surface roughness in the three-way simulation. The three-way experiment showed the lowest correlation coefficient (0.80; Table 1), the largest RMSE ($9.6\,m\,s^{-1}$) and the greatest variability of all the experiments. As we stated, model results are sensitive to parameterization of the surface roughness in wave-coupled models, an important factor in coupled TC modeling that deserves more research.

4.2. In Situ Comparisons of SST and Wave Height

Comparisons between simulated and observed SST and wave height time series were also used to evaluate model performance. The five buoys selected (shown in Figure 1a) featured data over the entire storm event with minimal gaps. Three buoys were chosen to the south and two to the north of the storm track in order to discern any along-shelf bias. Only the model experiments with time-dependent variables were considered for these comparisons (i.e., the WRF-Static experiment was excluded from the SST comparison and the three-way coupled experiment was the only simulation used for wave height comparison). Statistical analysis to

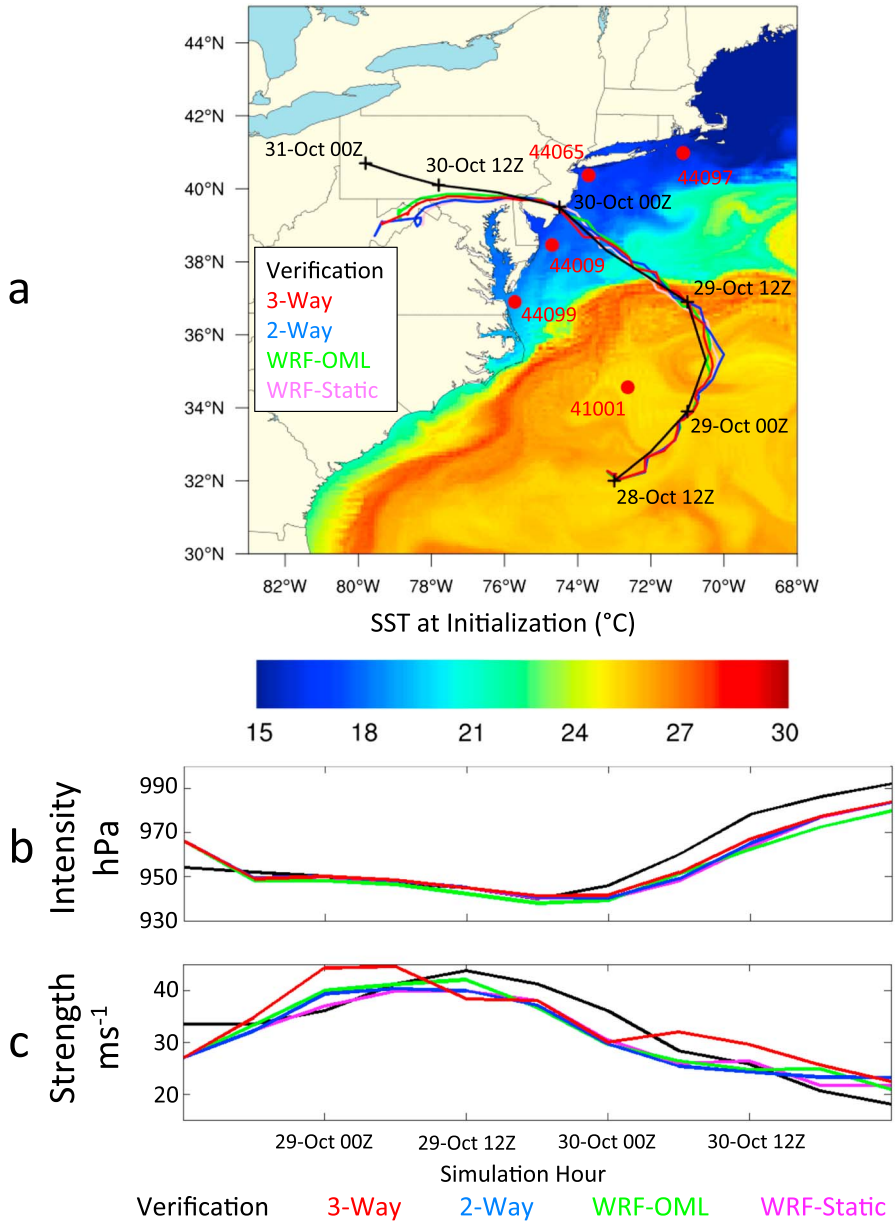

Figure 1. Comparison of Sandy's modeled track with (a) initial SST, (b) Sandy's intensity (minimum SLP), and (c) strength (maximum 10 m wind). Analysis completed from start of simulation (12Z 28 October) through dissipation (00Z 31 October). Panels include NHC best track Verification (black) and model experiments: three-way (red), two-way (blue), WRF-OML (green), and WRF-Static (magenta). Also shown are buoy locations (red dots, top panel) for time series analysis in Figure 2.

Table 1. Correlation Coefficient (*r*) and Root-Mean-Square Error (RMSE) of Four Experiments (Static, WRF-OML, Two Way, and Three Way) Compared to NHC's Best Track for Simulated Intensity (Minimum SLP; hPa) and Strength (Maximum 10 m Wind; m s^{-1}) of Sandy[a]

		Static	WRF-OML	Two Way	Three Way
r	Intensity	0.92	0.91	0.92	0.94
	Strength	0.94	0.90	0.90	0.80
RMSE	Intensity (hPa)	8.0	9.0	7.5	6.9
	Strength (m s^{-1})	6.3	7.2	7.5	9.6

[a]The temporal bounds of this comparison are from initialization (12Z 28 October) through termination of NHC's best track (00Z 31 October).

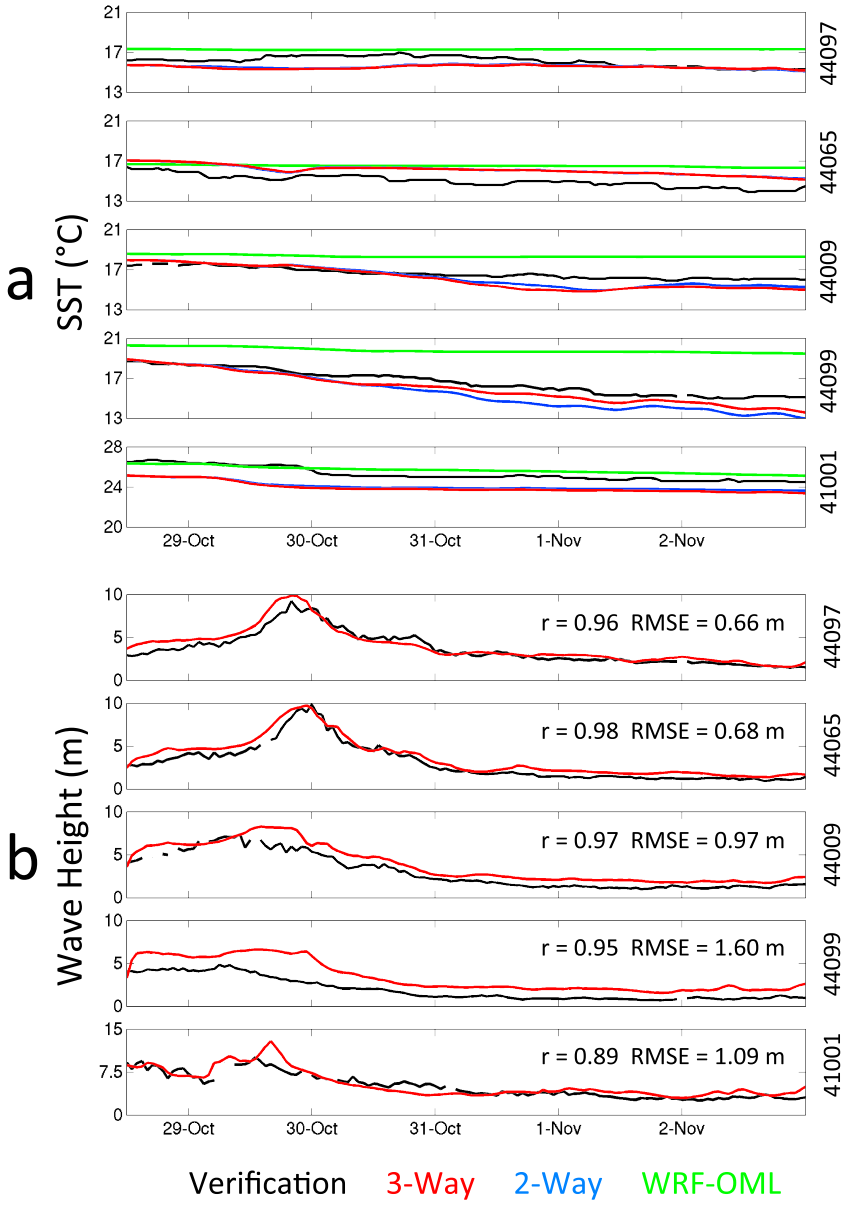

Figure 2. Time series comparison of Verification and model predictions of (a) SST (a) and of significant (b) wave height throughout the simulation (12Z 28 October through 00Z 3 November). Numbers are five near-shore buoys mapped in Figure 1a. SST time series includes three-way (red), two-way (blue), and WRF-OML (green) experiments. Significant wave height time series includes three-way case and modeled depth at buoy locations, along with associated correlation coefficient (*r*) and RMSE values. RMSE and *r* are calculated hourly for a total of 133 temporal points at each buoy (where in situ data are available). Verification for both time series is shown in black.

determine the correlation coefficient and RMSE were completed over the entire simulation (12Z 28 October through 00Z 3 November). This resulted in 133 temporal points of comparison at each buoy, although some small gaps from missing in situ data are present.

For the SST analysis (Figure 2a), the worst performing simulation was the WRF-OML, with an average correlation coefficient at all four locations of 0.62 and RMSE of 1.70°C. The two-way and three-way cases performed similarly to each other, with average correlation coefficients of 0.85 and 0.81 and RMSE of 0.98 and 0.96°C, respectively. At the buoy well to the south of the storm track (44,099), the two-way and three-way simulations had correlation coefficients of 0.99 and 0.98, and RMSE values of 1.17 and 0.71°C, respectively. At this location, the three-way simulation performed markedly better than the two-way experiment.

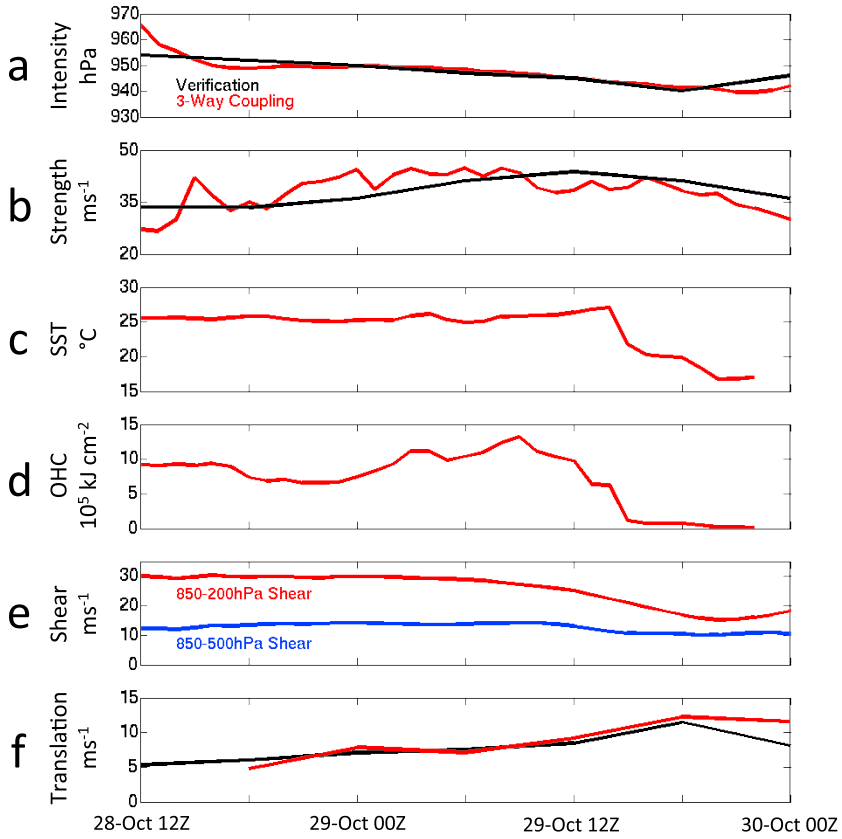

Figure 3. Environmental conditions prior to Sandy's landfall (12Z 28 October through approximately 00Z 30 October). Figure includes (a) simulated intensity (minimum SLP, hPa) every 3 h, (b) simulated strength (maximum 10 m wind, m s^{-1}) every 3 h, (c) hourly SST (°C), (d) hourly ocean heat content (OHC, 10^5 kJ cm^{-2}), (e) hourly vertical shear (m s^{-1}) calculated between 850/200 hPa (red) and 850/500 hPa (blue), and (f) translation speed (m s^{-1}) evaluated every 6 h. The three-way case was analyzed with NHC best track Verification (black) every 6 h.

Significant wave height comparisons showed good agreement with buoy data at the three northern stations, suggesting the three-way coupled simulation provided an excellent wavefield as Sandy moved onshore (Figure 2b). The worst comparison was at buoy 44,099, located farthest south from the storm track. At this location, the correlation coefficient was still good: 0.95. However, the model overestimated the waves with the RMSE of 1.60 m. The resolution of the ocean grid (7 km), plus unresolved nearby shoreline and the shallow depth (18.35 m), is likely culprits for the deficiency at this location. The best performing location was at buoy 44,097, the farthest to the northeast and the deepest (50.83 m), where the correlation coefficient was 0.96 and RMSE was 0.66 m.

4.3. Analysis of the Environmental Conditions Before Landfall

A number of marine environmental variables of potential importance to tropical and extratropical cyclones were examined (Figure 3). Observations were not available consistently, as remote-sensed or in situ data were missing during the storm (e.g., satellite SST data obscured by cloud cover). Our three-way coupling experiment provided temporally and spatially continuous modeled data time series for analysis. This analysis began at model initialization (12Z 28 October) and continued until just after landfall (00Z 30 October).

As we did to determine our simulated storm track, we used positions for the grid points of lowest sea level air pressure to determine the locations of the storm center, then extracted SST, ocean heat content (OHC) and vertical wind shear at these locations to examine how they changed as the storm center moved (Figure 3) from open ocean to the coast. OHC was calculated using a formula similar to [*Leipper and Volgenau*, 1972]:

$$\mathrm{OHC} = \rho c_p \int_{T=16^{\circ}\mathrm{C}} [T(z) - 16] \partial z$$

where ρ =1025 kg m^{-3}, c_p = 3850 J kg^{-1} °C^{-1}, and temperature anomaly (relative to 16°C) is integrated with depth relative to the 16°C isotherm. The 26°C isotherm used in *Leipper and Volgenau* [1972] was too warm for our analysis, as underlying SST during Sandy repeatedly fell below this value after Sandy crossed the Gulf Stream. In addition, we followed the method of *Rhome et al*. [2006] to calculate the atmosphere shear values: an annulus around the storm center was created, with an inner radius of 200 km and an outer radius of 800 km. The vertical vector differences of the annulus at two levels were then used to compute the shear. In particular, we analyzed the shear between 850 and 500 hPa, i.e., $\left|\overrightarrow{U}_{850-500}\right| = \left|\overrightarrow{U}_{850} - \overrightarrow{U}_{500}\right|$ [*Rhome et al*., 2006] as well as between 850 and 200 hPa, i.e., $\left|\overrightarrow{U}_{850-200}\right| = \left|\overrightarrow{U}_{850} - \overrightarrow{U}_{200}\right|$ [*Emanuel et al*., 2004], as both have been demonstrated to correlate well with time-dependent variations in storm intensity (minimum SLP) and strength (maximum 10 m wind). The translation speeds were estimated using the model-simulated and NHC-observed tracks until after Sandy made landfall, when the center of rotation became less well defined.

The minimum SLP simulated by the three-way coupled model and the Verification minimum SLP (Figure 3a) both demonstrate a slow increase until 5.5 h before landfall (2330Z 29 October) [*Blake et al*., 2013]. The three-way simulation resolved landfall about 1.5 h earlier. NHC best track wind speed gradually increased, peaked at 12Z 29 October (11.5 h before landfall), and then declined as the storm exited the Gulf Stream, made landfall, and headed inland (Figures 2b and 2c). SST at the storm center stayed relatively constant (~25°C) as Sandy moved from the Sargasso Sea and crossed the Gulf Stream. This is shown spatially at model initialization in Figure 1a and track following in Figure 3c. The sharp decline of SST occurred as the storm center moved west of the Gulf Stream and encountered cooler shelf water approximately 12 h before landfall. Correspondingly, the OHC (Figure 3d) at the storm center increased steadily as Sandy moved over the Sargasso Sea and Gulf Stream waters, then decreases sharply as it entered the shelf waters.

Concurrent with the gradual decrease in minimum SLP (Figure 3a) and increase in maximum wind speed (Figure 3b), both shear parameters (Figure 3e) gradually decreased (more subtle for the 850–500 hPa shear parameter) until just prior to landfall. As the storm moved across the coastal ocean, interaction with an upper level trough approaching the East Coast of the U.S. [*Blake et al*., 2013; *Galarneau et al*., 2013; *Shen et al*., 2013; *Munsell and Zhang*, 2014] resulted in the significant deep-layer shear present in our simulations. The presence of this deep-layer shear with continued intensification confirms the assertions of *Galarneau et al*. [2013]. Increasing baroclinicity and frontogenesis were keys to the secondary intensity maximum shortly before landfall. Before landfall, the storm was nontropical to the extent that the substantial vertical shear would not be expected to cause weakening.

The translation speed (Figure 3f) almost doubled (from 5 m s^{-1} to 10 m s^{-1}) until just prior to landfall, resolved in both the three-way simulation and the NHC best track. As a result of increased translation speed of Sandy, among the aforementioned uncoupled processes [*Galarneau et al*., 2013; *Shen et al*., 2013; *Munsell and Zhang*, 2014], the effect of a cooler SST was negligible toward the minimum SLP and maximum winds of the storm in the hours leading up to landfall.

5. Discussion and Conclusion

Superstorm Sandy made its way up the coast as a hurricane, interacting with ocean features in the Sargasso Sea, Gulf Stream, and shelf waters of the western North Atlantic Ocean before transitioning into an extratropical system. Utilizing the COAWST modeling system to quantify evolutions of marine environmental changes during this transition, we found that, regardless of coupling complexity, model-simulated tracks were all similar to the observations, suggesting the storm track was largely determined by large-scale synoptic atmospheric circulation, rather than by local processes resolved through model coupling. The translation speed also significantly increased (doubled) as Sandy moved across the shelf. As a result, ocean coupling did not have a drastic effect on simulated intensity and strength.

Relatively speaking, including the wave coupling in the three-way (ocean-atmosphere-wave) coupled configuration produced the most significant differences in the storm strength (maximum wind) comparisons. These differences were attributed to the atmospheric boundary layer interactions with surface roughness, calculated with consideration to wave heights. More research on wave-induced surface roughness parameterizations is needed.

Comparisons between simulated and observed SST and wave height time series at five buoys located on the U.S. mid-Atlantic coastal shelf showed the simulation of WRF coupled to a simple 1-D ocean mixed layer model had the largest errors. The three-way ocean-atmosphere-wave coupled model reproduced well the observed wave heights at three of the four locations; the one outlier was located in the shallowest water and closest to shore. A higher grid resolution ocean/wave model is needed to better resolve the wave dynamics there.

Together, the environmental conditions of Sandy prior to its landfall demonstrate that decreasing SST and OHC directly below the eye contributed to the storm losing its tropical characteristics several days prior to landfall. Despite that, Sandy had slight increases in strength (maximum winds) and intensity (minimum SLP) concurrent with reduced atmospheric shear as it accelerated toward the coastline while becoming a powerful extratropical system. Such a tropical-to-extratropical transition is crucial for storm classification during landfall, because the difference between naming a storm a hurricane or an extratropical cyclone has great implication for insurance claims. More research and observations are needed to better characterize the tropical to extratropical transition process of future storms similar to Sandy.

Acknowledgments

Research support provided by USGS Coastal Process Project, NOAA grant NA11NOS0120033, and NASA grant NNX13AD80G is much appreciated. We thank G. Lackmann for insightful discussions and J. Warrillow for her editorial assistance. Two anonymous reviewers also provided many constructive suggestions that helped us improve this manuscript. We acknowledge National Hurricane Center for making hurricane best track data available online.

The Editor thanks two anonymous reviewers for their assistance in evaluating this paper.

References

Beven, J. L., II (2012), Hurricane Sandy forecast discussion 19, Natl. Hurricane Cent., Miami, Fla. [Available at http://www.nhc.noaa.gov/archive/2012/al18/al182012.discus.019.shtml.]

Blake, E. S., T. B. Kimberlain, R. J. Berg, J. P. Cangialosi, and J. L. Beven II (2013), Tropical cyclone report: Hurricane Sandy, *Rep. AL182012*, Natl. Hurricane Cent., Miami, Fla.

Booij, N., R. C. Ris, and L. H. Holthuijsen (1999), A third-generation wave model for coastal regions: 1. Model description and validation, *J. Geophys. Res.*, *104*(C4), 7649, doi:10.1029/98JC02622.

Chassignet, E. P., H. E. Hurlburt, O. M. Smedstad, G. R. Halliwell, P. J. Hogan, A. J. Wallcraft, R. Baraille, and R. Bleck (2007), The HYCOM (HYbrid Coordinate Ocean Model) data assimilative system, *Marine Environmental Monitoring and Prediction Selected papers from the 36th International Liège Colloquium on Ocean Dynamics 36th International Liège Colloquium on Ocean Dynamics*, *65*, 60–83, doi:10.1016/j.jmarsys.2005.09.016.

Chen, F., and J. Dudhia (2001), Coupling an advanced land surface–hydrology model with the Penn State–NCAR MM5 modeling system. Part I: Model Implementation and Sensitivity, *Mon. Weather Rev.*, *129*(4), 569–585, doi:10.1175/1520-0493(2001)129<0569:CAALSH>2.0.CO;2.

Davis, C., et al. (2008), Prediction of landfalling hurricanes with the advanced hurricane WRF model, *Mon. Weather Rev.*, *136*, 1990–2005, doi:10.1175/2007MWR2085.1.

Drennan, W. M., P. K. Taylor, and M. J. Yelland (2005), Parameterizing the sea surface roughness, *J. Phys. Oceanogr.*, *35*, 835–848, doi:10.1175/JPO2704.1.

Dudhia, J. (1989), Numerical study of convection observed during the winter monsoon experiment using a mesoscale two-dimensional model, *J. Atmos. Sci.*, *46*(20), 3077–3107, doi:10.1175/1520-0469(1989)046<3077:NSOCOD>2.0.CO;2.

Emanuel, K. (2005), Increasing destructiveness of tropical cyclones over the past 30 years, *Nature*, *436*, 686–688, doi:10.1038/nature03906.

Emanuel, K., C. DesAutels, C. Holloway, and R. Korty (2004), Environmental control of tropical cyclone intensity, *J. Atmos. Sci.*, *61*, 843–858, doi:10.1175/1520-0469(2004)061<0843:ECOTCI>2.0.CO;2.

Flather, R. A. (1976), A tidal model of the northwest European continental shelf, *Mem. Soc. R. Sci. Liége*, *10*(6), 141–164.

Galarneau, T. J., Jr., C. A. Davis, and M. A. Shapiro (2013), Intensification of Hurricane Sandy (2012) through extratropical warm core seclusion, *Mon. Weather Rev.*, *141*, 4296–4321, doi:10.1175/MWR-D-13-00181.1.

Gopalakrishnan, S. G., S. Goldenberg, T. Quirino, X. Zhang, F. Marks Jr., K.-S. Yeh, R. Atlas, and V. Tallapragada (2012), Toward improving high-resolution numerical hurricane forecasting: Influence of model horizontal grid resolution, initialization, and physics, *Weather Forecasting*, *27*, 647–666, doi:10.1175/WAF-D-11-00055.1.

Haidvogel, D. B., et al. (2008), Ocean forecasting in terrain-following coordinates: Formulation and skill assessment of the regional ocean modeling system, *J. Comput. Phys.*, *227*, 3595–3624, doi:10.1016/j.jcp.2007.06.016.

Halliwell, G. R., Jr., L. K. Shay, J. K. Brewster, and W. J. Teague (2011), Evaluation and sensitivity analysis of an ocean model response to Hurricane Ivan, *Mon. Weather Rev.*, *139*, 921–945, doi:10.1175/2010MWR3104.1.

Hill, K. A., and G. M. Lackmann (2009), Influence of environmental humidity on tropical cyclone size, *Mon. Weather Rev.*, *137*, 3294–3315, doi:10.1175/2009MWR2679.1.

Hong, S.-Y., and J.-O. J. Lim (2006), The WRF single-moment 6-class microphysics scheme (WSM6), *J. Korean Meteor. Soc*, *42*, 129–151.

Janjić, Z. I. (1990), The step-mountain coordinate: Physical package, *Mon. Weather Rev.*, *118*(7), 1429–1443, doi:10.1175/1520-0493(1990)118<1429:TSMCPP>2.0.CO;2.

Janjić, Z. I. (1996), The surface layer in the NCEP Eta Model, *Eleventh Conference on Numerical Weather Prediction*, Norfolk, VA, 354–355, Am. Meteorol. Soc., Boston, Mass., 19–23 Aug.

Janjić, Z. I. (2002), Nonsingular implementation of the Mellor–Yamada level 2.5 scheme in the NCEP Meso model, *NCEP Office Note*, *437*, 61.

Kain, J. S. (2004), The Kain-Fritsch convective parameterization: An update, *J. Appl. Meteorol.*, *43*, 170–181.

Kirby, J. T., and T.-M. Chen (1989), Surface waves on vertically sheared flows: Approximate dispersion relations, *J. Geophys. Res.*, *94*(C1), 1013–1027, doi:10.1029/JC094iC01p01013.

Komen, G. J., K. Hasselmann, and K. Hasselmann (1984), On the existence of a fully developed wind-sea spectrum, *J. Phys. Oceanogr.*, *14*(8), 1271–1285, doi:10.1175/1520-0485(1984)014<1271:OTEOAF>2.0.CO;2.

Leipper, D., and D. Volgenau (1972), Hurricane heat potential of the Gulf of Mexico, *J. Phys. Oceanogr.*, *2*(3), 218–224.

Madsen, O. S., Y.-K. Poon, and H. C. Graber (1988), Spectral wave attenuation by bottom friction: Theory, *Coastal Eng. Proc.*, *1*(21), doi:10.9753/icce.v21.

Marchesiello, P., J. C. McWilliams, and A. Shchepetkin (2001), Open boundary conditions for long-term integration of regional oceanic models, *Ocean Modell.*, *3*(1–2), 1–20, doi:10.1016/S1463-5003(00)00013-5.

Mellor, G. L., and T. Yamada (1982), Development of a turbulence closure model for geophysical fluid problems, *Rev. Geophys.*, *20*(4), 851–875, doi:10.1029/RG020i004p00851.

Merrill, R. T. (1984), A comparison of large and small tropical cyclones, *Mon. Weather Rev.*, *112*(7), 1408–1418, doi:10.1175/1520-0493(1984)112<1408:ACOLAS>2.0.CO;2.

Mlawer, E. J., S. J. Taubman, P. D. Brown, M. J. Iacono, and S. A. Clough (1997), Radiative transfer for inhomogeneous atmospheres: RRTM, a validated correlated-k model for the longwave, *J. Geophys. Res.*, *102*(D14), 16663, doi:10.1029/97JD00237.

Monin, A. S., and A. M. Obukhov (1954), Basic laws of turbulent mixing in the surface layer of the atmosphere, *Contrib. Geophys. Inst. Acad. Sci. USSR*, *151*, 163–187.

Munsell, E. B., and F. Zhang (2014), Prediction and uncertainty of Hurricane Sandy (2012) explored through a real-time cloud-permitting ensemble analysis and forecast system assimilating airborne Doppler radar observations, *J. Adv. Model. Earth Syst.*, 38–58, doi:10.1002/2013MS000297.

National Centers for Environmental Prediction, National Weather Service, NOAA, U.S. Department of Commerce (2000), NCEP FNL operational model global tropospheric analyses, continuing from July 1999, doi:10.5065/D6M043C6.

Nelson, J., and R. He (2012), Effect of the Gulf Stream on winter extratropical cyclone outbreaks, *Atmos. Sci. Lett.*, *13*, 311–316, doi:10.1002/asl.400.

Olabarrieta, M., J. C. Warner, B. Armstrong, J. B. Zambon, and R. He (2012), Ocean–atmosphere dynamics during Hurricane Ida and Nor'Ida: An application of the Coupled Ocean–Atmosphere–Wave–Sediment Transport (COAWST) modeling system, *Ocean Modell.*, *43-44*, 112–137, doi:10.1016/j.ocemod.2011.12.008.

Oost, W. A., G. J. Komen, C. M. J. Jacobs, and C. van Oort (2002), New evidence for a relation between wind stress and wave age from measurements during ASGAMAGE, *Boundary Layer Meteorol.*, *103*(3), 409–438, doi:10.1023/A%3A1014913624535.

Pollard, R. T., P. B. Rhines, and R. O. R. Y. Thompson (1972), The deepening of the wind-mixed layer, *Geophys. Fluid Dyn.*, *4*(1), 381–404, doi:10.1080/03091927208236105.

Rhome, J. R., C. A. Sisko, and R. D. Knabb (2006), On the calculation of vertical shear: An operational perspective, *Preprints*: *27th Conference on Hurricanes and Tropical Meteorology*.

Shen, B. W., M. DeMaria, J. L. F. Li, and S. Cheung (2013), Genesis of Hurricane Sandy (2012) simulated with a global mesoscale model, *Geophys. Res. Lett.*, *40*, 4944–4950, doi:10.1002/grl.50934.

Skamarock, W., J. Klemp, J. Dudhia, D. Gill, D. M. Barker, W. Wang, and J. G. Powers (2005), A description of the Advanced Research WRF Version 2, *Tech. Note NCAR/TN-468+STR*, 88.

Smith, G. B. (2012), Some insurance companies to Sandy victims: You are covered for hurricanes, not floods, *New York Daily News*, 23 Nov.

Taylor, P., and M. Yelland (2001), The dependence of sea surface roughness on the height and steepness of the waves, *J. Phys. Oceanogr.*, *31*, 572–590.

Warner, J. C., B. Armstrong, R. He, and J. B. Zambon (2010), Development of a Coupled Ocean–Atmosphere–Wave–Sediment Transport (COAWST) modeling system, *Ocean Modell.*, *35*, 230–244.